Modal theory of modified spontaneous emission of a quantum emitter in a hybrid plasmonic photonic-crystal cavity system

Mohsen Kamandar Dezfouli,[1,*] Reuven Gordon,[2] and Stephen Hughes[1]

[1]*Department of Physics, Engineering Physics and Astronomy, Queen's University, Kingston, Ontario, Canada K7L 3N6*
[2]*Department of Electrical and Computer Engineering, University of Victoria, Victoria, British Columbia, Canada V8W 3P2*

We present an intuitive and accurate modal description of the rich optical physics involved for quantum dipole emitters coupled to hybrid plasmonic photonic-cavity structures. A significant frequency dependence for the spontaneous emission decay rate of a quantum dipole emitter coupled to these hybrid structures is found. In particular, it is shown that a Fano-type resonance reported experimentally in hybrid plasmonic systems arises from a large interference between two dominant quasinormal modes of the systems in the frequency range of interest. The presented modal theory forms an efficient basis for modeling quantum light-matter interactions in these complex hybrid systems and also enables the quantitative prediction and understanding of both radiative and nonradiative coupling for a wide range of dipole positions.

I. INTRODUCTION

Plasmonic devices show great promise for applications in quantum photonics and sensing technologies [1–4], due in part to the strong local field confinement below the diffraction limit. However, metals naturally have Ohmic losses and one must characterize both radiative enhancement effects and Ohmic dissipation on an equal footing. Despite their material losses, metal dimer antennas can have good single photon output β factors (i.e., the fraction of the dipole-emitted radiated power available in the far field) of more than 60% [5,6], as well as support very strong spontaneous emission (SE) rate enhancements [5,7,8]. In addition, integration of plasmonic structures with photonic crystal (PC) cavity platforms has been shown to offer new possibilities [4,9–12] that can benefit both from the higher quality (Q) factor of the PC subsystem and the stronger field enhancements and tighter light confinement by the plasmonic subsystem. In particular, plasmonic devices offer an extremely wide spectral bandwidth compared to dielectric devices such as PC cavities, because they have intrinsically low Qs. Therefore, by coupling these two systems together, the possibility of introducing very fine spectral features within a broad operating band can be investigated and exploited. Unfortunately, the theoretical description of such hybrid devices is rather scarce and particularly complicated because the traditional single mode cavity models faild for a number of reasons. For example, the rich physics behind Fano-type resonances that have been seen in hybrid plasmonic cavity systems [9] needs to be explored in more details, and is not well understood. In addition, hybrid plasmonic systems bring together two completely different length scales: a nanometer sized metallic resonator and a micrometer sized photonic cavity. Modeling these complex devices is not trivial and it is highly demanding for the usual computational models because of the different spatial grid requirements. Moreover, hybrid plasmonic systems are intrinsically lossy and are subjected to open boundary conditions, causing various conceptual problems with the development of an intuitive

modal theory, which is the typical approach for dielectric cavity systems.

In this paper, we demonstrate and apply an elegant modal theory that allows one to accurately model the underlying light-matter interactions and helps to explain the underlying physics of the complex line shapes. For the cavity structure of interest, we introduce a hybrid system that consists of a gold dimer [5] placed on top of a nanobeam PC cavity [13] and show how one can achieve very strong manipulation of SE decay rate. Perturbative analysis of similar structures has been done
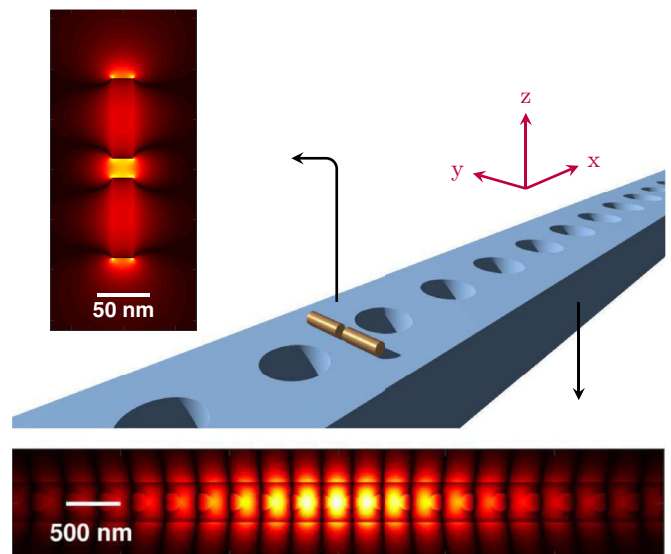

FIG. 1. Schematic of the hybrid device where a gold dimer of nanorods is placed on top of a nanobeam PC cavity. The top color map shows the $|E_y|^2$ of the dimer-only QNM in the middle of the dimer. The color map on the bottom shows the $|E_y|^2$ of the PC beam-only QNM in the middle of the slab. The QNM frequencies for the dimer and the PC cavity are $\tilde{\omega}_{\mathrm{di}}(\mathrm{eV}) = 1.7803 - 0.0678i$ and $\tilde{\omega}_{\mathrm{pc}}(\mathrm{eV}) = 1.6156 - 2.6908 \times 10^{-6}i$, respectively. The origin of our coordinate system, $(x,y,z) = (0,0,0)$, is placed exactly in the middle of the dimer gap which is 20 nm.

————
*Corresponding author: m.kamandar@queensu.ca

previously in order to estimate the frequency shift of the system resonances due to the interplay between the subsystems [14]; however, a full analytic characterization of the hybrid system using the system modes remains challenging. Using a rigorous modal description, we show that when a dipole (or single quantum emitter) is placed in between the dimer, then a significant interference between the quasinormal modes (QNMs) [15] of the two "cavities" takes place. The QNMs are the frequency domain mode solutions to the electromagnetic wave equation with open boundary conditions [16]. Using this modal description, we study how the Purcell factor and β factor changes as a function of frequency and dipole position and verify the accuracy of our approach against full dipole solutions to Maxwell's equations. This modal description not only explains the underlying physics of optical enhancement and quenching in these complex systems, but it can also be used as a foundation of studying quantum plasmonics in hybrid systems, where the use of a Purcell factor and modal theory have been questioned [17]. Indeed, plasmonic devices have been recently proposed for use in enhanced Raman detection experiments [18], where a suitable quantum mechanical description must be used [18,19]. This requires critical parameters such as the system losses that are typically included in a phenomenological manner. In contrast, our modal description paves the way toward building self-consistent quantum theories for hybrid plasmonic systems.

A schematic of the proposed device is shown in Fig. 1, where two color maps show the spatial profile of the main QNM of the individual subsystems, namely the gold dimer (top) and the nanobeam PC cavity (bottom). The dominant response of the combined system is driven by the two hybridized QNMs that are partly dimerlike and partly PC-like, as will be shown later. Since the two QNMs of interest strongly overlap in frequency, we employ a frequency domain technique [20] to calculate them, using the commercial software COMSOL. It should be noted that, the approach taken here in calculating and employing the QNMs is quite robust when different types of plasmonic and photonic cavities are used. However, adopting our theory in its current form to include the coupling to photonic waveguide modes is not straightforward, and is left to future work.

This paper is organized as follows. In Sec. II, the key elements of the QNM theory used to describe the radiative and nonradiative decay rates are presented. Next, in Sec. III, the details of the cavity system implementation are given, accompanied by the detailed confirmation of the accuracy of our model in predicting the correct electrodynamical response of the hybrid system when the PC and metal are strongly coupled near resonance. We find a significant change in the Purcell factor caused by modal interference, and we study how this factor changes as a function of dipole position. In Sec. IV, we also investigate an intermediate coupling regime, where the PC cavity resonance is detuned from the plasmon resonance by a few hundred meV, and demonstrate the accuracy of our approach in this regime as well. Section V is devoted to studying the nonradiative decay rates of the hybrid structures with the QNM approach, where again excellent agreement against full dipole numerical calculations are obtained using only the dominant two QNMs of the system. Finally, we present our conclusions in Sec. VI.

II. QUASINORMAL MODE THEORY OF ENHANCED SPONTANEOUS EMISSION FACTORS AND NONRADIATIVE DECAY

In general, for a medium described by the complex permittivity function $\varepsilon(\mathbf{r},\omega)$, the system Green function is defined as the solution to a point dipole that satisfies

$$\nabla \times \nabla \times \mathbf{G}(\mathbf{r},\mathbf{r}';\omega) - k_0^2\varepsilon(\mathbf{r},\omega)\mathbf{G}(\mathbf{r},\mathbf{r}';\omega) = k_0^2\delta(\mathbf{r}-\mathbf{r}')\mathbf{I},$$
(1)

where, $k_0 = \omega/c$ is the free space propagation constant and $\mathbf{I}$ is the unity dyadic. In addition, the system QNMs, $\tilde{\mathbf{f}}_\mu(\mathbf{r})$, are solutions to a non-Hermition Maxwell's problem that are associated with a complex eigenfrequency $\tilde{\omega}_\mu = \omega_\mu - i\gamma_\mu$, the imaginary part of which is a measure of energy leakage. The non-Hermiticity originates from the fact that the system QNMs are solutions to Helmholtz equation

$$\nabla \times \nabla \times \tilde{\mathbf{f}}_\mu(\mathbf{r}) - \frac{\tilde{\omega}_\mu^2}{c^2}\varepsilon(\mathbf{r},\omega)\tilde{\mathbf{f}}_\mu(\mathbf{r}) = 0,$$
(2)

subjected to open boundary condition [21]. The system response can be analyzed in the basis of the QNMs through the Green function expansion [22]:

$$\mathbf{G}^{\mathrm{QNM}}(\mathbf{r},\mathbf{r}';\omega) = \sum_\mu \frac{\omega^2}{2\tilde{\omega}_\mu(\tilde{\omega}_\mu - \omega)}\tilde{\mathbf{f}}_\mu(\mathbf{r})\tilde{\mathbf{f}}_\mu(\mathbf{r}'),$$
(3)

when the selected QNMs are dominantly contributing over the frequency region of our interest. In order for the correct physical quantities such as Purcell factor to be obtained from this Green function expansion, normalized QNMs must be used. Normalization of the QNMs is not a trivial task but can be done in different ways [23,24], where, in general, spatial integration of the QNMs over the computational volume is involved. However, following [20], we avoid the difficulties of spatially integrating QNMs and rather use the dipole response at its own location to obtain the normalized QNMs from the Green function expansion. The procedure is such that, first, one needs to perform an iterative search for the QNM frequency of the interest by looking at the hybrid system response; because the QNMs are the pole of the system Green function, the closer one gets to the QNM frequency the stronger the response will become. Once the QNM frequency is found, one needs to perform two separate dipole calculations, one in the presence of the hybrid system and one in free space, in order to obtain the scattered field from the hybrid geometry. Since the scattered field is obtained at the QNM frequency, its contribution is dominantly that particular QNM. We did a careful analysis of mesh elements and open boundary conditions to ensure convergent results. For our calculations, we use approximately 840 000 total number of elements, simulation volume of 6 μm^3, with 10 PML layers, where the underlying symmetry of the system was used to reduce the computational resources needed.

Associated with this general non-Hermitian theory, there is also a complex mode volume for QNMs that can be defined from [21,23,24]

$$V_\mu^{\mathrm{QNM}} = \frac{1}{n_b^2\tilde{\mathbf{f}}_\mu^2(\mathbf{r}_\mathrm{c})},$$
(4)

where n_b is the refractive index of the background medium where the dipole emitter is embedded, and $\mathbf{r}_c$ is the characteristic position of a dipole emitter that will be coupled to the QNM (i.e., typically at a local field maximum). The usual *real-valued* effective mode volume for use in the conventional Purcell's equation is defined via [23]

$$\frac{1}{V_\mu^{\text{eff}}} = \text{Re}\left\{\frac{1}{V_\mu^{\text{QNM}}}\right\}. \qquad (5)$$

Aside from being complex, the generalized mode volume in (4) can also be negative in complex system where multiple resonances are involved [25] as we will also see later.

The QNM expansion of the Green function can then be used to obtain the SE decay rate of a quantum dipole emitter, $\mathbf{d} = d\,\mathbf{n}$, oriented along $\mathbf{n}$ direction and placed at some position $\mathbf{r}_d$, through

$$\Gamma(\mathbf{r}_d) = \frac{2}{\hbar\varepsilon_0}\,\mathbf{d}\cdot\text{Im}\{\mathbf{G}^{\text{QNM}}(\mathbf{r}_d,\mathbf{r}_d;\omega)\}\cdot\mathbf{d}. \qquad (6)$$

If using the Green function for the homogeneous medium, $\mathbf{G}^{\text{B}}$, where $\mathbf{n}\cdot\text{Im}\{\mathbf{G}^{\text{B}}(\mathbf{r}_d,\mathbf{r}_d;\omega)\}\cdot\mathbf{n} = \omega^3 n_b/6\pi c^3$, one can easily calculate the free space SE decay rate, Γ_0, and therefore compute at the projected SE enhancement factor along the dipole direction:

$$F(\mathbf{r}_d) = \frac{\Gamma(\mathbf{r}_d)}{\Gamma_0}, \qquad (7)$$

which is a generalized Purcell factor. In addition, the QNMs of the system can be used to calculate the nonradiative decay rate of the same dipole using [26]

$$\Gamma_{\text{NR}}(\mathbf{r}_d) = \frac{2}{\hbar\omega\varepsilon_0}\int_V \text{Re}\{\mathbf{j}(\mathbf{r})\cdot\mathbf{E}^*(\mathbf{r})\}d\mathbf{r}, \qquad (8)$$

where $\mathbf{E}(\mathbf{r}) = \mathbf{G}^{\text{QNM}}(\mathbf{r},\mathbf{r}_d;\omega)\cdot\mathbf{d}$ is the field emitted by the dipole at $\mathbf{r}_d$ and $\mathbf{j}(\mathbf{r}) = \varepsilon_0\,\omega\,\text{Im}\{\varepsilon(\mathbf{r})\}\mathbf{E}(\mathbf{r})$ is the current density induced by the dipole over the metal volume, V. Therefore, this spatial integral can be used to compute the Ohmic losses in a given problem. Accordingly, the ratio between the radiated power to the far field and the total radiated power by the dipole is given by the single photon β factor (or quantum efficiency of the emitter),

$$\beta(\mathbf{r}_d) = 1 - \frac{\Gamma_{\text{NR}}(\mathbf{r}_d)}{\Gamma(\mathbf{r}_d)}. \qquad (9)$$

Similar to the Purcell factor calculations, full-dipole numerical calculation of the β factor usually requires performing tedious numerical simulations per source point (e.g., for each dipole position) of interest. However, once the system QNMs are computed (as a function of space), the analytical spatial integration in Eq. (8) provides the nonradiative decay properties of the system over a wide range of spatial positions and frequencies, using only the discrete QNMs of interest. This latter approach is naturally orders of magnitude faster than full dipole calculations, and also helps to explain the underlying physics.
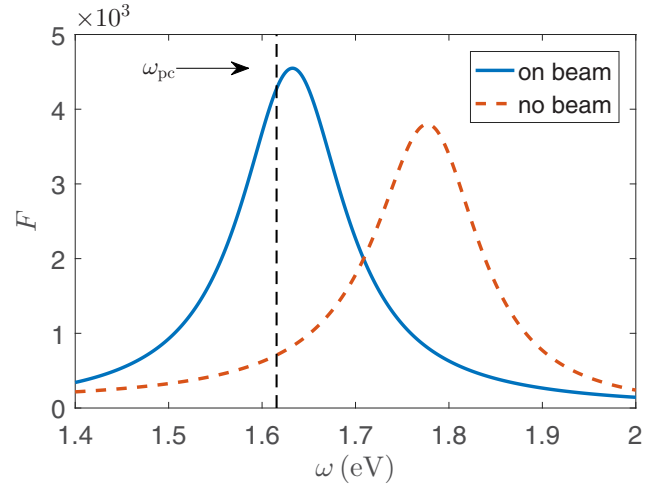

FIG. 2. Comparison between the Purcell factor, F, of a y-polarized dipole placed in between the gold nanorods (center position), when in free space (dashed red) and when placed on top of the dielectric beam (5 nm away from the beam surface) without any PC holes (solid blue).

III. GOLD DIMER STRONGLY COUPLED TO PC NANOBEAM

Gold dimer resonators can be designed to have both high a Purcell factor and a high β factor, as discussed in the Introduction [5]. In this work, we consider a dimer made of two gold nanorods with radius of $r_{\text{Au}} = 10$ nm and rod height of $h_{\text{Au}} = 80$ nm, respectively. The dimer is assumed to be in free space with background refractive index of $n_b = 1$. To simulate the gold dispersive behavior, the usual Drude model is used

$$\varepsilon(\omega) = 1 - \frac{\omega_{\text{p}}^2}{\omega(\omega + i\gamma_{\text{p}})}, \qquad (10)$$

where $\omega_{\text{p}} = 1.26 \times 10^{16}$ rads/s is the plasma frequency and $\gamma_{\text{p}} = 1.41 \times 10^{14}$ rads/s is the collision rate. This particular dimer has a single mode behavior over a wide range of frequencies as shown in Fig. 2, with the peak localized plasmon resonance appearing near 1.8 eV. The dimer alone has a very large $F = 3800$, caused by coupling to the mode profile shown in Fig. 1, when the dipole is placed in the middle of the dimer gap and oriented along the y direction. If one brings the gold dimer close to the surface of a nanobeam without any PC structure patterned (i.e., a beam without holes), there will be two main effects: the resonance frequency of the dimer is redshifted and the decay rate becomes enhanced further. This is shown in the same figure for comparison, when the gold dimer is placed 5 nm away from the surface of the beam. The accurate knowledge of the spectral redshifting is clearly important in obtaining good coupling between the two subsystems.

The nanobeam PC cavity is modeled as silicon nitride, with a refractive index of $n = 2.04$ [27]. The height and the width of beam are $h = 200$ nm and $w = 367$ nm, respectively. Following [27], the nanobeam design includes two sections, namely a mirror and taper region, where the hole radius and spacing are different. The taper section is made of seven holes, such that their radius were decreased from 86 nm to 68 nm and their spacing was decreased from 306 nm to

264 nm, in a linear fashion. On the ends of the taper section, the mirror section is designed such that 17 holes of fixed radius $r = 86$ nm with fixed spacing of $a = 306$ nm are used. The length of the cavity region in between the two smallest holes, in the very middle of the structure, is chosen to be 126 nm. This design supports one main QNM of interest at $\tilde{\omega}_c(\text{eV}) = 1.6156 - 2.6908 \times 10^{-6}i$, corresponding to a large quality factor of $Q = 3 \times 10^5$. The mode profile for this QNM is also shown in Fig. 1. Our investigations show that this PC cavity supports additional QNMs at lower frequencies with lower Qs that can be effectively ignored for working in the frequency range of our interest; this will be made clearer when discussing the F characteristics of the device below.

When the gold dimer is placed on top of the nanobeam cavity, the individual modes discussed above become strongly hybridized. The resonance frequencies of the two hybridized QNMs are $\tilde{\omega}_1(\text{eV}) = 1.6429 - 0.0548i$ and $\tilde{\omega}_2(\text{eV}) = 1.6063 - 0.0144i$, corresponding to $Q_1 = 15$ and $Q_2 = 55$, respectively. Notice the Fano feature associated with the second QNM d gives rise to the interesting interference feature in the total decay behavior of the quantum emitter placed in the middle of the dimer gap. Although such features have been seen before [9], they lack a quantitative theoretical description. Fano type resonances appear many different plasmonic systems with application ranging from lasing to switching [28,29], where many of them the can be modelled using our presented theory. Our approach, can be also applied to a wide range of photonic cavity structures including inverse photonic structures [30]. The associated generalized mode volumes at $\mathbf{r}_0$ are also estimated to be $V_1^{\text{QNM}}(\lambda_1{}^3) = (1.96 + 0.68i) \times 10^{-4}$ and $V_2^{\text{QNM}}(\lambda_2{}^3) = (-0.86 - 6.39i) \times 10^{-4}$. Note that the latter is negative which originates from the interference between two subsystems and can be understood by looking at the actual contributions from each QNM to the total decay rate of the dipole; being negative suggests that this volume does not represent a physical volume, but rather is a quantity with dimensions of volume required for use in the calculation of the Purcell factor. Note that, when there is only one QNM present in a system, or when the QNMs are sufficiently far apart in frequency such that strong interference features are not seen, then the V^{QNM} becomes positive and can be interpreted as the conventional mode volume. Similar mode volumes have been previously reported for coupled metallic rods [24] and for coupled cavities in PCs [24,25].

The two coupled QNMs are believed to be responsible for the dominant response of the system over the frequency range of interest. In order to confirm this and represent the accuracy of the analytical model in the basis of QNMs, the predicted F is compared with the dipole calculations. In Fig. 3, F is plotted using dipole calculations in circles and analytic calculations in solid line, where an excellent agreement between the two is obtained. In the same figure, we have also plotted the contributions from each individual mode. Note that each of the individual enhancement factors do not necessarily represent physically meaningful quantities; however, the total enhancement is confirmed to be always positive and well behaved. There are also small oscillations present in the full-dipole calculations at lower frequencies that are not captured by the analytic model, since we only use a
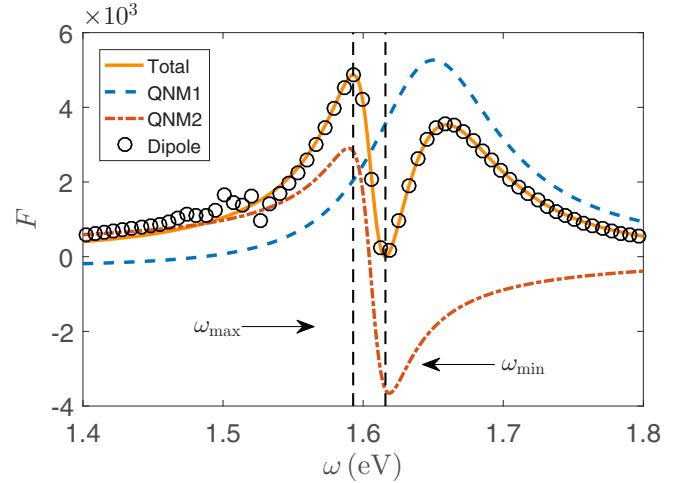

FIG. 3. Generalized Purcell factor, F, calculated for the hybrid structure where the y-polarized excitation dipole is placed at $(x,y,z) = (0,0,0)$ (see Fig. 1). The solid orange line is the analytic calculation using an expansion of the dominant QNMs of the system, while the black circles are the full dipole calculations. The small disagreement at lower frequencies comes from other QNMs of the PC cavity that are not included in the two-QNM analytical study.

two mode expansion. As mentioned before, these are due to contributions from lower frequency modes of the PC cavity and can be safely ignored (though they could be included if more modes were deemed necessary). The two QNM modal description provides an accurate model to the full system response including the enhanced decay rate of a given dipole at various locations over a wide range of frequencies, where normally one single dipole calculation must be performed per frequency point per spatial position. In addition, as will be discussed next, the modal expansion brings new insights into the underlying physics that is not normally available from full dipole calculations. Worth to note is that the same Green function of the hybrid system can then be used to explore the quantum dynamics of quantum emitters coupled to this system [31].

The maximum modal SE enhancement is approximately $F = 4900$ which is similar to that achieved using the dimer on top of the slab alone. However, this maximum now occurs at a different frequency closer to the frequency of higher-Q QNM which itself is near the resonance of the bare PC cavity. This accurate knowledge of the frequency shifting, which is a consequence of an effective coupling between the two components of the hybrid device, is well beyond weak coupling. But, more importantly, just next to the maximum, as a result of the very strong interference between the two individual QNMs, a minimum enhancement occurs that is drastically different in magnitude compared to the maximum; indeed the F is significantly reduced (approximate to $F = 4$), which can potentially be utilized as a switching mechanism between the two fundamentally different response regimes of the system. For example, a quantum dot placed in the dimer gap will become relatively dark if excited at this particular frequency, whereas in contrast becomes quickly bright when one moves away from this minimum point.
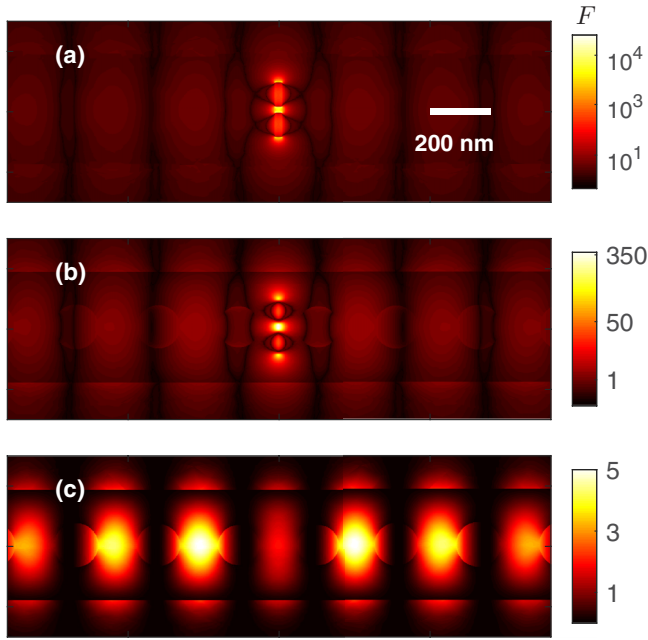
FIG. 4. (a)–(c) Generalized Purcell factor, F, at $z = 0$ (in between the dimer gap), $z = -15$ nm (at the beam surface) and $z = -115$ nm (in the middle of the beam), respectively. Since the field intensity around dimer is orders of magnitude larger than in PC beam, a nonlinear scale is used to better highlight the spatial mode features.

As mentioned earlier, hybrid QNMs of the system inherit features from both the dimer and PC cavity. However, the low-Q mode is more dimerlike than the high-Q mode. Indeed, for the particular structure under study, the magnitude of the field in between dimer gap is found to be more than an order of magnitude stronger than in the center of the nanobeam, for both of the QNMs, which is another indication of significant hybridization of the individual QNMs of the system. To help quantify the hybrid characteristics of these modes, it is useful to look at a spatial map of the enhancement factor, F. In Fig. 4, we plot F at three different heights (z values) over a rectangular xy cut: (a) at the center of the dimer, (b) on the surface of the nanobeam, and (c) at the nanobeam center. Note that the system response behaves mostly dimerlike in Fig. 4(a), whereas in contrast becomes more PC cavity like in Fig. 4(c). However, at any height both components contribute to the response. These maps are calculated at the frequency of the maximum enhancement factor in Fig. 3, shown by the dashed line. A drastic decrease in d F is seen when moving away from dimer and closer to the nanobeam, as shown in Fig. 3. However, this trend is not always obtained and depending on frequency, e.g., at the exact frequency that the minimum takes place, we found that quite the opposite occurs and F will increase from its minimum value in the dimer gap to higher values in the middle of the nanobeam. This is a nontrivial feature of this hybrid device that originates from significant hybridization discussed earlier. It should be also noted that, because the dimer greatly shapes the structures of both of the QNMs in this device, the increase in d F mentioned later is not as drastic as the decrease in the previous scenario.
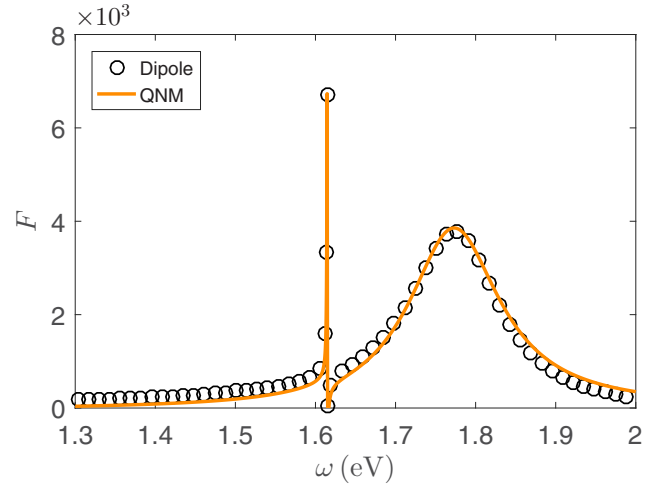

FIG. 5. Generalized Purcell factor, F, calculated for the second hybrid structure where the gold dimer is moved further away from the PC nanobeam by 100 nm compared to the initial configuration for the strong coupling (which causes a detuning of the QNMs by around 160 meV). Similar to before, a y-polarized excitation dipole is placed at the middle of the dimer gap. The solid line is the analytic calculation using an expansion of the two dominant QNMs of the system, while the circles are the full dipole calculations.

IV. INTERMEDIATE COUPLING REGIME

The strong interference discussed so far is considered when the individual resonances are very close in frequency such that the significant reduction in the emission enhancement at the plasmonic resonances is seen. Whether the present modal theory can predict the correct physics involved in hybrid structures at other frequency regimes where the PC resonance is coupled to the plasmonic tail rather than the plasmonic peak, might be questioned. To address this question, we now consider another hybrid device where the dimer is spatially shifted 100 nm above the PC nanobeam and as a result the coupling between plasmonic and photonic resonances occurs at the tail of the plasmonic mode, in a much weaker coupling regime. Once again we employ a two QNMs expansion of the Green function in order to study this weak coupling regime. The new resonances in for this configuration are $\tilde{\omega}_1$(eV) $= 1.7719 - 0.0691i$ for the dimerlike QNM and $\tilde{\omega}_2$(eV) $= 1.6147 - 0.0003i$ for the PC-like QNM. These, translate to $Q_1 = 13$ and $Q_2 = 2400$ for the dimerlike and the PC-like QNMs, respectively. Note that the plasmonic quality factor is almost the same, whereas the PC quality factor is greatly enhanced. This is characteristic of the intermediate coupling where the PC resonance is less affected (broadened) by the presence of the gold dimer. In Fig. 5, we show the comparison between our modal calculation (in solid) and the full dipole calculation (in circles) of the SE enhancement, where an excellent agreement is once again obtained. Moreover, we show a wider range of frequencies in order to show the degree of accuracy in the QNM prediction of the enhancement emission at frequencies farther away from the plasmonic resonance. This is quite remarkable given the fact that QNMs are evaluated at one single frequency and then used to obtain the hybrid system response at far

detuned frequencies. Also, in this new configuration, the contribution from other PC resonances, that were seen before, are less noticeable. This is indeed expected as now these other resonances are coupled farther down the tail of the plasmonic QNM, where comparably a less efficient coupling will occur. Another important point to make is that the highest emission enhancement takes place near the PC-like QNM of the system and is indeed higher than the maximum enhancement possible near the plasmonic dimer (and even using the plasmonic dimer on its own when there is no PC present). Most certainly, this enhancement is lowered compared to the bare PC cavity, but the benefits of the plasmonic dimer can now be exploited. Given the fact that QNMs are extremely less computationally expensive to calculate compared to full dipole calculation, it is clear that this modal theory presents both a rigorous and economical tool for studying such plasmonic hybrid systems.

V. NONRADIATIVE DECAY RATES

As for any plasmonic device, achieving a high emission enhancement for a quantum emitter placed in proximity of the metal is not good enough on its own, as one also needs to know how much of this value is quenched. Indeed, a good portion of the SE enhancement is due to the coupling to the induced charges in the form of Ohmic losses. Therefore, it is essential to quantify the nonradiative contribution to the decay rate, Γ_{NR}, that can be computed analytically using the system QNMs. Employing Eq. (8) is trivial in the case of a single mode system, as one has to perform a simple spatial integration of the system QNM over the metallic region. However, extra care must be taken when there are two (or more) QNMs involved. In the present case, we have two QNMs dominantly responsible for the emitter behavior and therefore the field generated over the lossy region has dominant contributions from both of these QNMs, i.e., where

$$\mathbf{E}(\mathbf{r}) = \frac{\omega^2 \tilde{\mathbf{f}}_1(\mathbf{r}_0) \cdot \mathbf{d}}{2\tilde{\omega}_1(\tilde{\omega}_1 - \omega)} \tilde{\mathbf{f}}_1(\mathbf{r}) + \frac{\omega^2 \tilde{\mathbf{f}}_2(\mathbf{r}_0) \cdot \mathbf{d}}{2\tilde{\omega}_2(\tilde{\omega}_2 - \omega)} \tilde{\mathbf{f}}_2(\mathbf{r}). \quad (11)$$

Thus there will be cross-coupling of the two QNMs of the hybrid system to be integrated over the metallic region. In contrast to the total decay rate, F, simply adding contributions from single QNMs do not add up to the total Γ_{NR}. Note that additional QNMs can, in principle, also contribute to the nonradiative decay rate through a spatial integral involving the dominant QNMs of the system. However, as will be shown below, the two-QNM Green function indeed also gives a very good agreement against full dipole calculations for the Γ_{NR}.

In Fig. 6, we plot the Γ_{NR} for the hybrid system where the general trend of the total nonradiative decay rate is similar to the total decay rate. In the same figure, we have also plotted the pure modal contributions to the nonradiative decay rate form each QNM. Note that these do not represent physically meaningful quantities on their own, and adding them together will not provide the interference feature associated with the true nonradiative decay behavior. However, as discussed earlier, the cross term contribution is essential to explain the correct physics of nonradiative decay.

Finally, we also investigate the validity of our modal nonradiative decay rates by calculating the Γ_{NR} for the second configuration of the hybrid plasmonic device discussed in
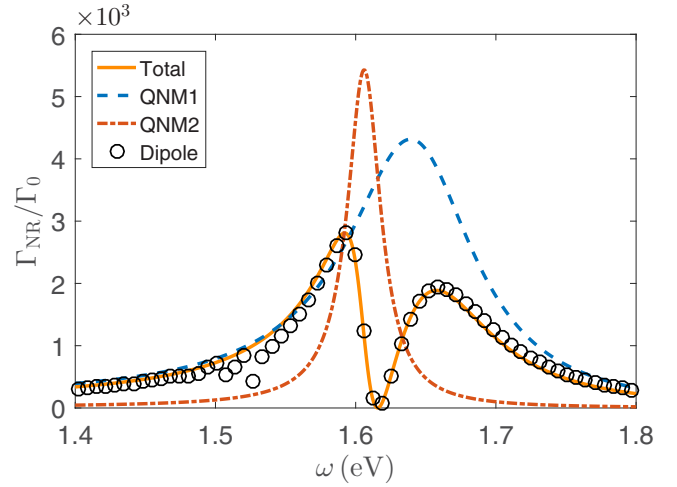

FIG. 6. Nonradiative decay rate, Γ_{NR}, calculated for the hybrid structure where the excitation dipole is placed at $(x,y,z) = (0,0,0)$ (see Fig. 1). This corresponds to the emission enhancement plot shown in Fig. 3. The solid orange line is the analytic calculation using a Green function expansion in terms of dominant QNMs of the system, while the black circles are the full dipole calculations. Some small discrepancies at lower frequencies come from other QNMs of the PC cavity that are not included in the two mode expansion.

Sec. IV. The result for this comparison is plotted in Fig. 7 over a wide range of frequencies, where an excellent qualitative agreement is shown.

Our analysis in this section shows a relatively fixed beta value of approximately $\beta = 0.46$ for the first configuration of the hybrid plasmonic device with near resonance coupling, and a relatively fixed value of approximately $\beta = 0.4$ for the second configuration with the off-resonance coupling, over a
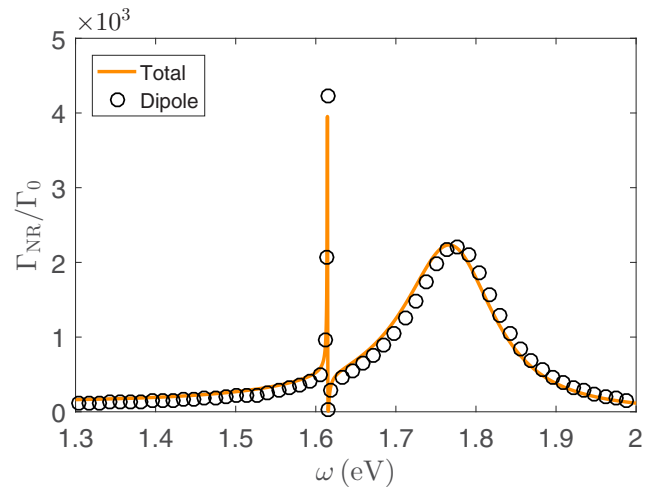

FIG. 7. Nonradiative decay rate, Γ_{NR}, calculated for the second hybrid structure where the gold dimer is moved further away form the PC nanobeam by 100 nm compared to the initial configuration used for the strong coupling. This corresponds to the emission enhancement plot shown in Fig. 5. The solid line is the analytic calculation using a Green function expansion of the system response in terms of dominant QNMs of the system, while the circles are the full dipole calculations.

wide range of frequencies. It is interesting that the stronger interference effects that are present in the first hybrid device also facilitate more output power of the coupled dipole.

VI. CONCLUSION

In conclusion, we have introduced a hybrid plasmonic-PC system that is capable of very strong modification of the SE decay rate of dipole emitters when placed right in the middle of the dimer gap. The drastic change from $F = 4900$ to $F = 4$ can be utilized as a switching knob to trigger into fundamentally different response regimes of this system. In addition, the overall β factor (or quantum efficiency) of about 0.46 is achieved that suggests reasonable output coupling of the light to the far field. To study the system in detail, we have adopted a QNM description that is capable of presenting a clear and intuitive picture of the complex physics behind the nontrivial dipole response. With this efficient

modal description, the full decay SE rate characteristics of the system are quickly available, which can also be used to study quantum light-matter interactions, when quantum emitters such as quantum dots are coupled to these hybrid systems. Moreover, this analytical QNM approach allows one to compute the nonradiative coupling (frequently ignored in the literature) to the underlying QNMs, which is essential for designing and optimizing such structures for use in emerging nanophotonics technologies.

[1] K. Kneipp, Y. Wang, H. Kneipp, L. T. Perelman, I. Itzkan, R. R. Dasari, and M. S. Feld, Phys. Rev. Lett. **78**, 1667 (1997).

[2] K. A. Willets and R. P. V. Duyne, Annu. Rev. Phys. Chem. **58**, 267 (2007).

[3] R. Zhang, Y. Zhang, Z. C. Dong, S. Jiang, C. Zhang, L. G. Chen, L. Zhang, Y. Liao, J. Aizpurua, Y. Luo, J. L. Yang, and J. G. Hou, Nature (London) **498**, 82 (2013).

[4] M. D. Baaske and F. Vollmer, Nat. Photon. **10**, 733 (2016).

[5] R.-C. Ge and S. Hughes, Opt. Lett. **39**, 4235 (2014).

[6] L. Rogobete, F. Kaminski, M. Agio, and V. Sandoghdar, Opt. Lett. **32**, 1623 (2007).

[7] K. J. Russell, T.-L. Liu, S. Cui, and E. L. Hu, Nat. Photon. **6**, 459 (2012).

[8] E. J. R. Vesseur, F. J. G. de Abajo, and A. Polman, Phys. Rev. B **82**, 165419 (2010).

[9] M. Barth, S. Schietinger, S. Fischer, J. Becker, N. Nüsse, T. Aichele, B. Löchel, C. Sönnichsen, and O. Benson, Nano Lett. **10**, 891 (2010).

[10] A. E. Eter, T. Grosjean, P. Viktorovitch, X. Letartre, T. Benyattou, and F. I. Baida, Opt. Express **22**, 14464 (2014).

[11] Y.-F. Xiao, Y.-C. Liu, B.-B. Li, Y.-L. Chen, Y. Li, and Q. Gong, Phys. Rev. A **85**, 031805 (2012).

[12] H. M. Doeleman, E. Verhagen, and A. F. Koenderink, ACS Photon. **3**, 1943 (2016).

[13] I. Mukherjee, G. Hajisalem, and R. Gordon, Opt. Express **19**, 22462 (2011).

[14] I. Mukherjee and R. Gordon, Opt. Express **20**, 16992 (2012).

[15] P. T. Kristensen and S. Hughes, ACS Photon. **1**, 2 (2014).

[16] P. T. Leung, S. Y. Liu, and K. Young, Phys. Rev. A **49**, 3982 (1994).

[17] A. F. Koenderink, Opt. Lett. **35**, 4208 (2010).

[18] P. Roelli, C. Galland, N. Piro, and T. J. Kippenberg, Nat. Nano **11**, 164 (2016).

[19] M. K. Schmidt, R. Esteban, A. González-Tudela, G. Giedke, and J. Aizpurua, ACS Nano **10**, 6291 (2016).

[20] Q. Bai, M. Perrin, C. Sauvan, J.-P. Hugonin, and P. Lalanne, Opt. Express **21**, 27371 (2013).

[21] P. T. Kristensen, R.-C. Ge, and S. Hughes, Phys. Rev. A **92**, 053810 (2015).

[22] K. M. Lee, P. T. Leung, and K. M. Pang, J. Opt. Soc. Am. B **16**, 1409 (1999).

[23] P. T. Kristensen, C. Van Vlack, and S. Hughes, Opt. Lett. **37**, 1649 (2012).

[24] C. Sauvan, J. P. Hugonin, I. S. Maksymov, and P. Lalanne, Phys. Rev. Lett. **110**, 237401 (2013).

[25] J. R. de Lasson, P. T. Kristensen, J. Mørk, and N. Gregersen, Opt. Lett. **40**, 5790 (2015).

[26] P. Anger, P. Bharadwaj, and L. Novotny, Phys. Rev. Lett. **96**, 113002 (2006).

[27] M. W. McCutcheon and M. Lončar, Opt. Express **16**, 19136 (2008).

[28] B. Luk'yanchuk, N. I. Zheludev, S. A. Maier, N. J. Halas, P. Nordlander, H. Giessen, and C. T. Chong, Nat. Mater. **9**, 707 (2010).

[29] H. Chen, S. Liu, J. Zi, and Z. Lin, ACS Nano **9**, 1926 (2015).

[30] J. Du, S. Liu, Z. Lin, J. Zi, and S. T. Chui, Phys. Rev. A **83**, 035803 (2011).

[31] R.-C. Ge and S. Hughes, Phys. Rev. B **92**, 205420 (2015).